university of groningen

University Medical Center Groningen

University of Groningen

Low energy electrodynamics of high Tc superconductors

Feenstra, Bokke Johannes

IMPORTANT NOTE: You are advised to consult the publisher's version (publisher's PDF) if you wish to cite from it. Please check the document version below.

Document Version
Publisher's PDF, also known as Version of record

Publication date:
1997

Link to publication in University of Groningen/UMCG research database

Citation for published version (APA):
Feenstra, B. J. (1997). *Low energy electrodynamics of high Tc superconductors*. s.n.

Copyright
Other than for strictly personal use, it is not permitted to download or to forward/distribute the text or part of it without the consent of the author(s) and/or copyright holder(s), unless the work is under an open content license (like Creative Commons).

The publication may also be distributed here under the terms of Article 25fa of the Dutch Copyright Act, indicated by the "Taverne" license. More information can be found on the University of Groningen website: https://www.rug.nl/library/open-access/self-archiving-pure/taverne-amendment.

Take-down policy
If you believe that this document breaches copyright please contact us providing details, and we will remove access to the work immediately and investigate your claim.

Downloaded from the University of Groningen/UMCG research database (Pure): http://www.rug.nl/research/portal. For technical reasons the number of authors shown on this cover page is limited to 10 maximum.

Download date: 04-05-2023

Chapter 6

mm-Wave Transmission through Superconducting Thin Films

6.1 Introduction

Many of the contemporary results on the electrodynamical properties of high T_c superconductors in the microwave region have been obtained by exploiting resonant techniques such as cavity perturbation [1–3]. Although these techniques yield results having a very high accuracy, obtaining absolute quantities is rather difficult due to intrinsic experimental complications [4]. By measuring mm-wave transmission through a superconducting thin film one is able to obtain *absolute* information about both the real and the imaginary part of its dielectric function [5]. Already around the formulation of the BCS-theory [6], mm-wave and far infrared transmission through superconducting thin films was used as a sensitive technique to probe the energy gap, present in the excitation spectrum of conventional superconductors such as Pb and Al [7, 8].

We first demonstrate the principle of the transmission measurement by showing some examples in which the optical constants of some dielectric (substrate) materials are determined. In the sections thereafter we present the results of mm-wave transmission measurements performed on both conventional (MoGe, NbN) and a high temperature superconductor ($DyBa_2Cu_3O_{7-\delta}$). The conventional superconductors, the optical response of which is well-established, were mainly investigated in order to demonstrate that we are able to determine the intrinsic properties of the film. We will show the absolute magnitude of properties such as the penetration depth λ, the optical conductivity σ_1 and the permittivity ϵ', resulting from the analysis. In particular, in section 6.4 where we describe the results obtained on a series of $DyBa_2Cu_3O_{7-\delta}$ films with thicknesses ranging from 20 to 80 nm, special attention will be paid to the significance of the film thickness in mm-wave transmission measurements.

6.2 Dielectric Materials

In chapter 3 we have seen that due to the multiple reflections on each interface both the transmitted and the reflected signal from a layered material exhibits an interference pattern. An easy way to observe these interference effects is to measure the transmission of mm-waves through a plan-parallel dielectric material, which has a low absorption coefficient in this frequency range. By measuring the magnitude of the interference peaks and the distance between two adjacent peaks one can experimentally determine the complex dielectric function p of the dielectric, where $p = \eta + i\kappa$. The amplitude of the maxima is directly related to the degree of absorption within the material, κ, and has an optimal value of 1 for an absorptionless dielectric. The distance between two adjacent peaks is determined by the product *kpd*, where k is the wave vector, $2\pi\nu/c$ and d is the sample thickness. In our experiment k runs from 4 to 6 cm^{-1}. Since both k and d are known very precisely, one can determine the value for η.

Two examples of such interference patterns measured on fused quartz and KRS-5 can be seen in fig. 6.1. The solid lines are transmission coefficients calculated using the formulation

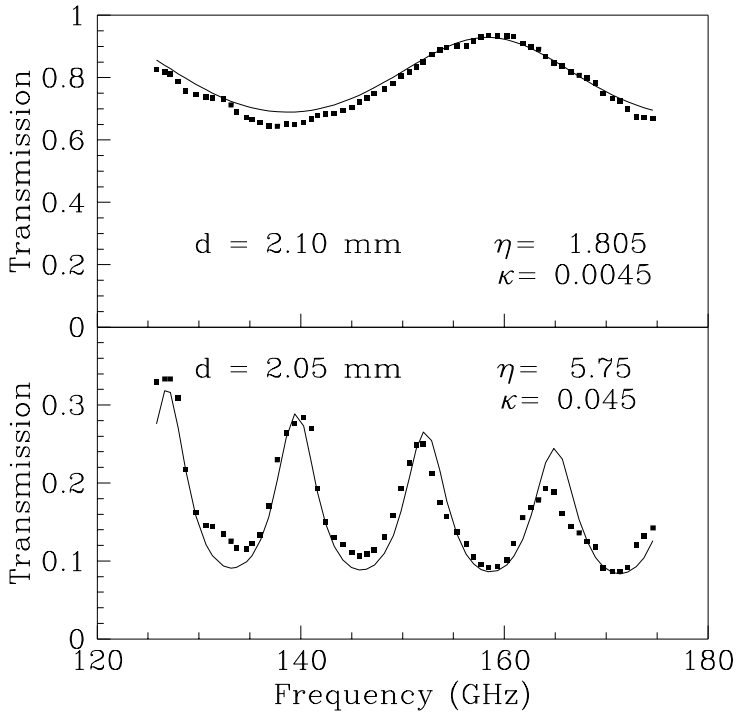

Figure 6.1: *Fabry-Perot resonance spectra for two commonly used window materials, fused quartz (top) and KRS-5 (bottom).*

presented in chapter 3 (see eq. 3.12). These two commonly used window materials show a very distinct response at these frequencies. Fused quartz is often employed as a window for mm-wave as well as MIR radiation, and shows a very high transmission over the entire

range, indicative of both a low absorption ($\kappa = 0.0045$) and a low index of refraction, $\eta = 1.805$. This small value is apparent from the distance between the maxima, which is rather large even though the thickness of the quartz sample is 2.10 mm. Moreover, also the high transmission in the minima indicates a small η.

The KRS-5 sample shows several peaks, while the thickness of the sample is the same, indicating that the index of refraction is much larger, $\eta = 5.75$. Also the absolute magnitude of the transmission over the entire range is much lower and the spectrum exhibits the "typical" tilted spectrum for a highly absorbing sample, having $\kappa = 0.045$.

In fig. 6.2 we show another example, the frequency response of two dielectrics commonly used as substrates for high T_c thin films, $LaAlO_3$ and $NdGaO_3$. Also in this case the Fabry-

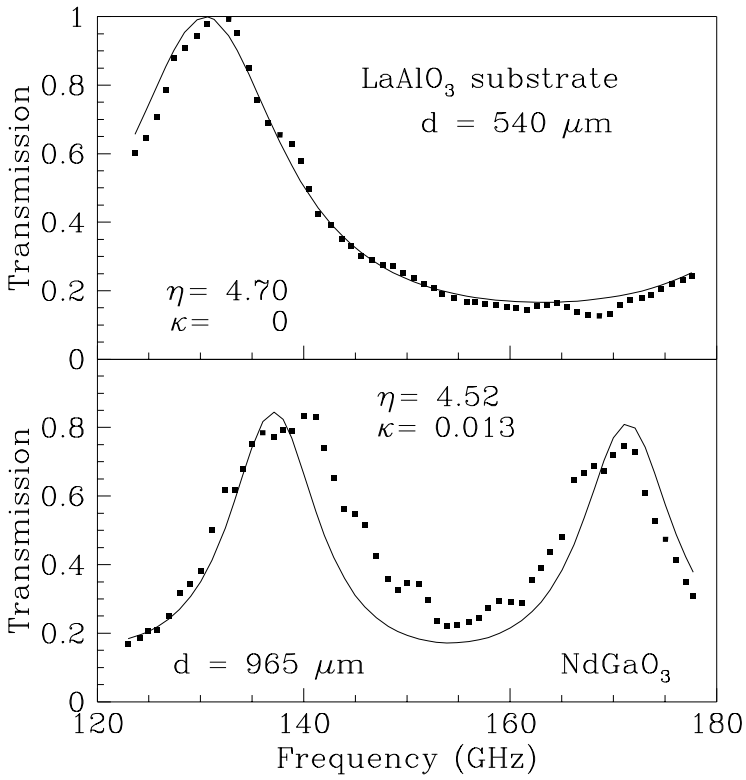

Figure 6.2: *Fabry-Perot resonance spectra for two perovskite substrate materials, $LaAlO_3$ (top) and $NdGaO_3$ (bottom).*

Perot resonances are well described by the calculated transmission. The response of the $NdGaO_3$ substrate was measured in the early stages of the setup, and therefore showssome remaining discrepancies due to diffraction and spurious leakage, while the $LaAlO_3$ substrate was measured more recently, clearly showing the improved performance. For $LaAlO_3$ the maximum transmission is equal to 1, manifesting that at these frequencies the absorption in this material can be neglected. From the period we obtain that $\eta = 4.70$. In the case

of $NdGaO_3$, the maximum amplitude is slightly reduced, suggestive of the presence of a small absorption. The fringes are closer together compared to the case of $LaAlO_3$ due to the larger thickness, since the important parameter determining the period is the product kpd. The obtained optical constants are $\eta = 4.52$ and $\kappa = 0.013$.

In the remainder of this chapter, the optical constants of the used substrate are always determined experimentally by the method described above. Also the temperature dependence of the optical constants is measured since the transmission of the bare substrate and film+substrate are measured subsequentially at a fixed temperature (see chapter 4).

6.3 Conventional Superconductors

In order to check the reliability of the technique, and the performance of our newly build setup, we began by measuring some conventional superconductors, exhibiting BCS-behavior. In doing so, we made sure that we are able to resolve the intrinsic properties of the superconducting thin film. In this section the results on two of these materials, MoGe and NbN, are presented.

6.3.1 MoGe

Introduction

The first example of mm-wave transmission experiments performed on a conventional superconductor were done using an 800 $\mathring{A}$ thick MoGe film, provided to us by Prof. S. M. Anlage. The film was deposited on the $<100>$ surface of a 520 μm thick Si substrate, by co-magnetron sputtering from single element sources at ambient temperature. The deposition was done in an Argon atmosphere, at a pressure of 5 mTorr. Rapid substrate rotation (3000 rpm) was used during deposition to improve the sample homogeneity and coverage.

MoGe, being an amporphous superconductor, combines microscopic disorder with a homogeneity on the length scale important for superconductivity (i.e. the coherence length ξ). It therefore attracted some attention in the early eighties, as a testcase to investigate the validity of theories developed at that time, concerning the influence of Anderson localization on superconductivity [9].

Moreover, due to the relatively large penetration depth ($\lambda(0) \sim 7000 - 7700\mathring{A}$ [10,11]) one can consider thin films having a thicknes upto several hundred $\mathring{A}$ as if they were essentially two-dimensional. This led for instance to the observation of a Kosterlitz-Thouless transition in thin (500-5000 $\mathring{A}$) a-MoGe films [10].

Due to the long penetration depth, along with the short coherence length ($\xi(0) = 55\mathring{A}$ [11]) MoGe can be classified as an extreme type II superconductor, similar as the high T_c's. Henceforth a renewed interest in thin MoGe layers, and multilayer structures using Ge as the intermediate layer, was initiated after the discovery of the high T_c compounds. Using artificial multilayer structures one is able to perform a range of experiments which are very difficult or even impossible to acchieve within a genuine high T_c superconductor. For instance, by changing the interlayer thickness, one can modify the Josephson coupling

between the superconducting layers and thus study the influence of the coupling on superconductivity. Also, due to the low dimensionality of the thin film, one can investigate the behavior of an individual layer independently. Furthermore, through the use of materials such as MoGe, in which the critical field, H_{c2} is considerably lower, one attain access to the entire H,T-phase diagram.

Main focus of the research on artificial layered structures has therefore been on studying the vortex dynamics. Important questions that are addressed are the number of different phases, their character and which of these phases exhibit zero resistivity. Using MoGe/Ge multilayers White *et al.* [11] and Steel *et al.* [12] were able to show the crossover from a region in which the vortices in one particular layer are coupled to the vortices in the adjacent layer, to a situation at higher temperatures and/or fields where the vortices are completely decoupled, i.e. 2-dimensional. A similar system was used to demonstrate that the existence of Josephson vortices in between the superconducting layers does not produce the (in)famous sign reversal in the vortex Hall effect [13].

In our case the main goal in studying MoGe was to establish whether we are able to probe the intrinsic BCS-properties of the thin film, using mm-wave transmission experiments.

Results

The critical temperature of the MoGe film was checked by dc-resistivity measurements, presented in fig. 6.3. The low temperature region has been expanded and can be seen in the inset. The dc-resistivity shows a nearly temperature independent behavior in the

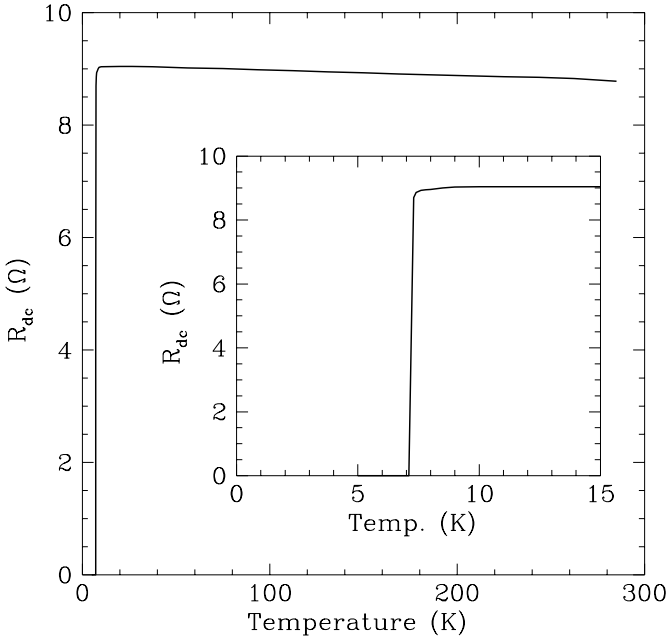

Figure 6.3: *dc-Resistivity measurements for an 800 Å thick MoGe film, deposited on a Si substrate.*

normal state, typical for such films. T_c is 7.2 K while the width of the transition is approximately 0.1 K. Plotted is the resistivity measured using a four-point measurement.

In fig. 6.4 the transmission through a bare Si-substrate is depicted. From this we

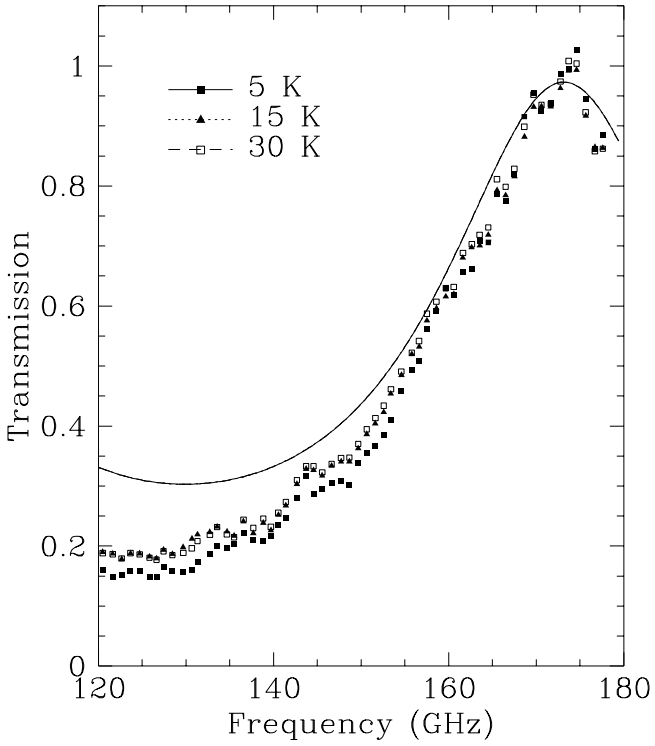

Figure 6.4: *Transmission through a bare Si substrate. The obtained optical constants are:* $\eta = 3.32$ *and* $\kappa = 0.004$.

obtained the optical constants for the substrate, $\eta = 3.32$ and $\kappa = 0.004$. We see that there is no temperature dependence in the range of interest, below 30 K. At higher temperatures the transmission started to be reduced due to thermally activated carriers, introduced by the inhomogeneties within the silicon. Using the experimentally determined optical constants of the substrate, we can model the transmission through the entire system, i.e. the MoGe thin film on a Si substrate.

The transmission coefficient has been depicted in fig. 6.5 as a function of frequency, for three different temperatures (4.5, 7.0 and 30 K, from bottom to top). In the normal state the absolute magnitude of the transmission is determined by the real part of the conductivity σ_1, which is nearly temperature independent. The best fit is obtained using $\sigma_1 = 17,300\ (\Omega\mathrm{cm})^{-1}$. This cannot be directly compared to the value obtained from the dc-resistivity, however, as we will also see in the next section, the magnitude is reasonable for such a film. Due to the high conductivity of the metallic film the interference pattern has been shifted compared to the observed spectrum for the bare substrate. Notice furthermore that the interference pattern shows no major changes besides the reduced amplitude upon entering the superconducting state. These phenomena will be treated in more detail in

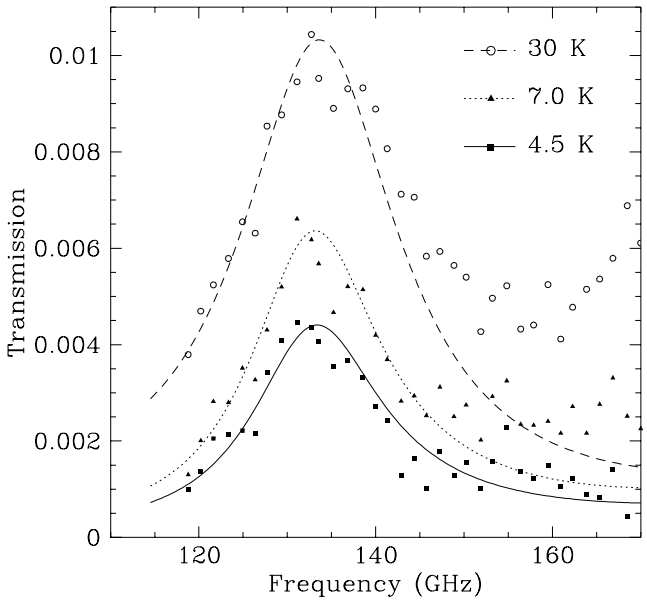

Figure 6.5: *Frequency dependence of the mm-wave transmission through a MoGe film on Si, plotted for several temperatures.*

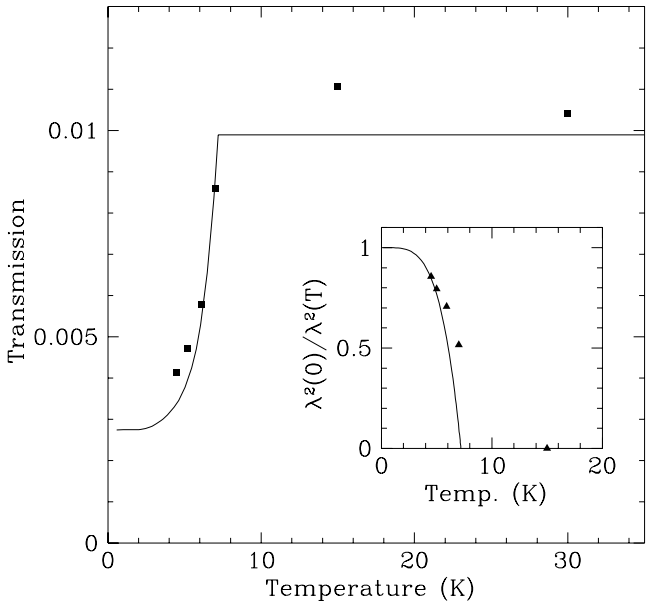

Figure 6.6: *Temperature dependence of the transmission through a MoGe film on a Si substrate along with the calculated transmission for a BCS-superconductor having* $\sigma(10) = 17,300(\Omega\text{cm})^{-1}$ *and* $\lambda(0) = 5000\mathring{A}$. *Inset: temperature dependence of the superfluid density compared to the BCS-prediction.*

section 6.4.

The discrepancy at higher freqencies can presumably be attributed to the presence of radiation traversing a different path. Its temperature dependence, resembling the temperature dependence of the superconducting thin film, is strong evidence against assigning this contribution to leakage radiation. If the beam would pass the sample under a nonzero angle of incidence, the effective thickness of the substrate would be larger, giving rise to additional peaks, most likely broadened, in the Fabry-Perot resonance pattern.

In the superconducting state we assume that the dielectric function of the thin film is dominated by the superfluid contribution, yielding an absolute value for the penetration depth, since $\lambda \sim 1/\omega_{ps}$. The lowest value obtained for the fit at 4.5 K is approximately 5410 $\mathring{A}$.

In fig. 6.6 the transmission is shown as a function of temperature, at a fixed frequency of 133 GHz. The reduction of transmission at T_c due to the strongly enhanced screening caused by the presence of the superfluid is evident. At the lowest temperature the transmission starts to level off, but still is not temperature independent, which indicates that the gap has not fully opened yet. The measured transmission agrees fairly well with the predicted BCS-behavior represented by the solid line. In the normal state a temperature independent σ_1 was used, having a value of 17,300 $(\Omega\text{cm})^{-1}$. In the superconducting state σ_1 vanishes according to the Mattis-Bardeen relations [14] and λ obeys [15]

$$\lambda(T) \;=\; \lambda(0)\left[1 \;-\; \left(\frac{T}{T_c}\right)^4\right]^{-1/2} \tag{6.1}$$

Using this temperature dependence we can also calculate the superfluid density n_s, according to $\lambda^2(0)/\lambda^2(T)$, taking $\lambda(0) = 5000\mathring{A}$. The agreement with the measured superfluid density has been shown in the inset of fig. 6.6. In addition we can see that the T_c of this material is too low to observe the temperature independence of λ, typical for a BCS-superconductor exhibiting activated behavior.

6.3.2 NbN

NbN is a conventional superconductor having a much higher critical temperature than MoGe. T_c can range from 16 upto 18 K by the inclusion of carbon. We measured the transmission of mm-waves through a 55 nm thick NbN film deposited on a 490 μm thick MgO substrate. The sample preparation has been described in chapter 5, where the same film was used to measure the transmission and reflection coefficient in the FIR-range.

In fig. 6.7 the dc-resistivity, R_{dc} has been plotted. The resistivity has a negative temperature coefficient observed more often for thin metallic films and shows a transition at starting at 17 K, having a width of approximately 0.8 K. The transmission through a bare MgO substrate, having a thickness of 640 μm, is shown in fig. 6.8. The obtained optical constants are $\eta = 3.43$ and $k = 0.006$. Please note that the thickness of the substrate used for the reference measurement is not the same as the one on which the NbN film was deposited. The possibility of using substrates of unequal thicknesses is given by the system of modeling the transmission through the complete stratified sample.

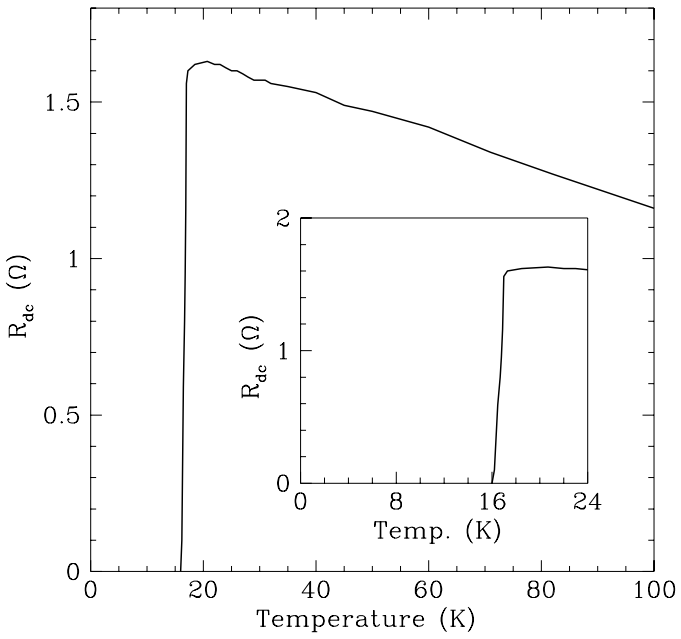

Figure 6.7: *dc-Resistivity measurements for a 55 nm thick NbN film, deposited on a MgO substrate.*

In fig. 6.9 the transmission through the NbN film on MgO is shown as a function of frequency, for several temperatures, both above and below T_c. The peak in the interference spectrum is determined by the MgO substrate. We are able to fit the spectra using the two fluid description of equation (3.25). As expected for a metallic film, $\epsilon'' \gg \epsilon'$, while in the superconducting state the opposite is valid, $\epsilon' \gg \epsilon''$. For the fit we have focused our attention on the main peak around 135 GHz. The poor fit at higher frequencies has the same origin as the discrepancies seen in the MoGe analysis. Also in this case the magnitude of the contribution follows the temperature dependence of the main peak. In later experiments the control over undesired reflections and standing waves was improved even further, thereby removing this phenomenon.

Plotting the temperature dependence at one particular frequency (140 GHz) as shown in fig. 6.10, the dramatic change in transmission at T_c is more easily observed. The temperature dependence of the transmission coefficient can be fitted very well using the assumptions that λ(T) can be described by the Gorter Casimir relation given in eq. (6.1), σ_1(T) follows the Mattis-Bardeen relations and $2\Delta\,/\,kT = 4.0$. The only adjustable parameters used in the calculation were the normal state conductivity ($\sigma_1\,(17K) = 15,000\ \Omega^{-1}\mathrm{cm}^{-1}$) determining the transmission at 17 K and the London penetration depth ($\lambda_L = 400$ nm) giving the transmission at low temperatures. Although this penetration depth is somewhat higher than the lowest reported values of about 100 nm [16], there is considerable variation in the literature due to a wide range of film structures.

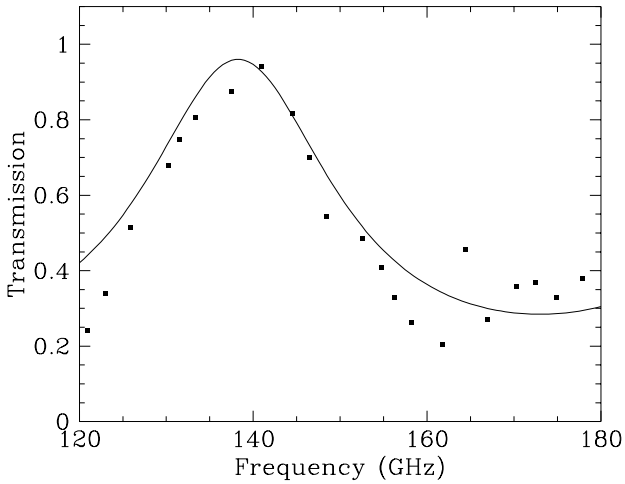

Figure 6.8: *Transmission through a bare MgO substrate. The obtained optical constants are: $\eta = 3.43$ and $\kappa = 0$.*

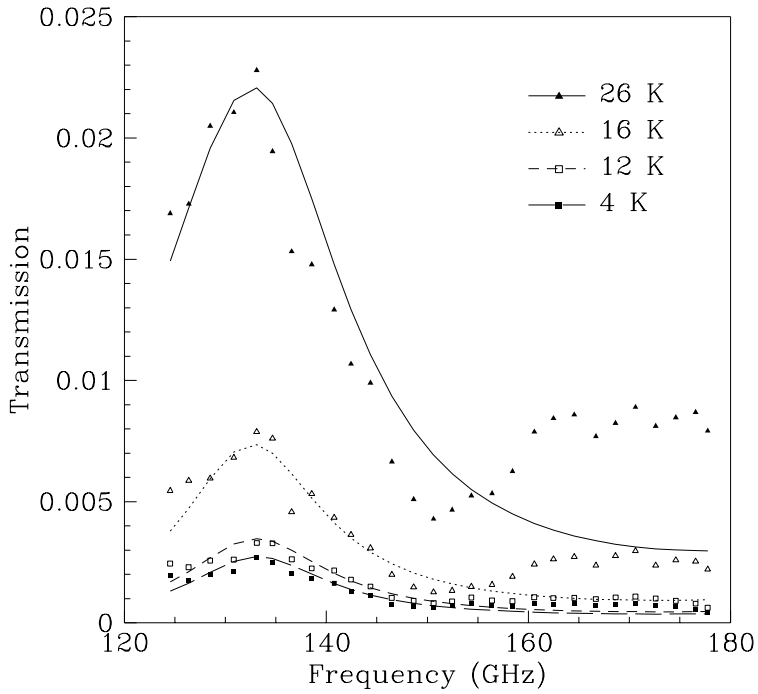

Figure 6.9: *Transmission of NbN on MgO (thickness = 55 nm, $T_c = 17$ K) for 4 different temperatures (4 K: solid squares, 12 K: open squares, 16 K: open triangles and 26 K: solid triangles) together with their fit. Inset: temperature dependence at 140 GHz together with a BCS-fit.*

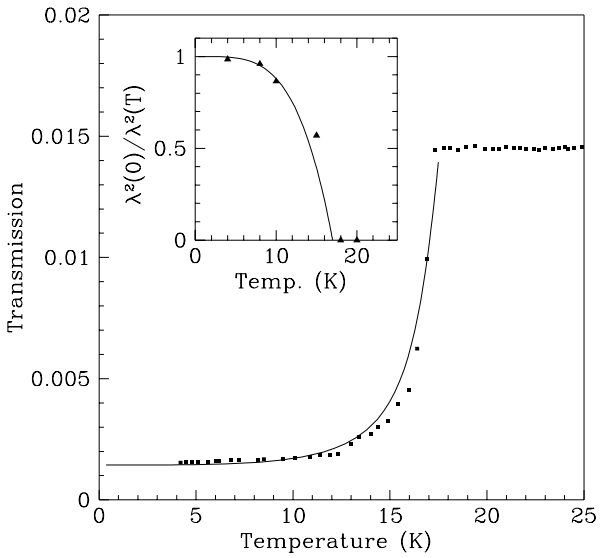

Figure 6.10: *Temperature dependence at 140 GHz together with a BCS-fit using* $\sigma_1(17K) = 15{,}000\ \Omega^{-1}cm^{-1}$ *and* $\lambda_L = 400\,nm$. *Inset: Temperature dependence of the superfluid density, along with the expected BCS-behavior.*

The conductivity agrees well with the value of 14,000 Ω^{-1}cm^{-1} given in chapter 5, which was obtained using FIR-spectroscopy. In contrast to the case of MoGe the temperature independence of the transmission coefficient, due to the exponential behavior of λ is clearly visible. In the inset of fig. 6.10 the superfluid density has been plotted along with its predicted behavior, showing a satisfactory agreement.

6.4 $DyBa_2Cu_3O_{7-\delta}$

Sample Preparation

The $DyBa_2Cu_3O_{7-\delta}$ films of thicknesses ranging from 20 to 80 nm, were deposited by RF sputtering on $LaAlO_3$ substrates using the (100) surface. The substrate temperature was 745 °C while a mixture of argon and oxygen gas was used, at pressures of 105 and 45 mTorr respectively. After the deposition the samples were annealed in 200 mTorr oxygen for 30 minutes at 450 °C. The quality of the surface was checked with X-ray diffraction, which showed a very good crystallization. Due to the high crystallinity of the films, the oxygen diffusion process was rather slow resulting in a somewhat reduced T_c (88 K) for one of the films (20 nm).

Transmission Results

In this section the influence of the thickness of the superconducting film on the mm-wave transmission, in particular its temperature dependence, will be presented. The results on a series of films, having a thickness ranging from 20 to 80 nm will be analyzed. We demonstrate that taking the film thickness into account is essential for obtaining the intrinsic temperature dependence of the material properties. Moreover, by selecting the right film thickness we are able to choose the sensitivity such that either the conductivity or the superfluid density ($\sim 1/\lambda^2$) dominates the temperature dependence of the transmission coefficient. We will show that for certain values of the London penetration depth λ_L and the normal state conductivity σ_n, one can choose the film thickness such that even in the superconducting state downto rather low temperatures ($\sim$ 60 K) the superfluid density appears to be absent.

In fig. 6.11 the transmission through a 20 nm thick $DyBa_2Cu_3O_{7-\delta}$ film on a $LaSrO_3$ substrate is shown. Similar results as presented below have been reproduced on a different batch of films. The interference pattern of the substrate at room temperature was shown already in fig. 6.2 in section 6.2, from which we obtained $\eta = 4.70$ and $\kappa = 0$. As expected the optical constants are temperature independent for the perovskite substrate. The additional oscillations present in the transmission are caused by internal reflections within the sampleholder. Due to the slightly modified standing wave pattern, these do not cancel completely after division by the transmitted signal through a reference hole.

In contrast to the results for the MoGe and the NbN film presented in the previous section, the interference pattern of the $DyBa_2Cu_3O_{7-\delta}$ thin film changes dramatically when the temperature is lowered. This is due to the stronger change in conductivity of the film, thereby altering the matching of the impedances of both film and substrate. This effect can be demonstrated by modeling the transmission through a similar stratified system, changing either the optical conductivity σ_1 of the film, keeping the thickness fixed at 20 nm (fig. 6.12a) or by altering its thickness at a fixed conductivity of 3000 $\Omega^{-1}\text{cm}^{-1}$ (fig. 6.12b). Both parameters will have a similar effect on the transmission since this is mainly affected by their product. For a certain set of parameters the interference effect disappears completely, showing that the light passes through the substrate only once. Additionally, the magnitude of the dielectric function matching this requirement determines the absolute value of transmission at the turning point.

This model calculation illustrates furthermore that one has to be careful with the interpretation of transmission curves measured as a function of temperature at a fixed frequency. A curve taken at 130 GHz will show a much larger temperature dependence than a curve taken at 150 GHz, although they will yield the same intrinsic film properties, once interference effects are taken into account. This effect is demonstrated in fig. 6.13, where we plotted the temperature dependence of the transmission through the $DyBa_2Cu_3O_{7-\delta}$ film, for several frequencies.

At 150 GHz the transmission is nearly constant at temperatures higher than 60 K. At lower temperatures the amplitude of the interference peak drops and its width decreases rapidly. The transmission for the 34 nm film is depicted in fig. 6.14 for the same tempera-

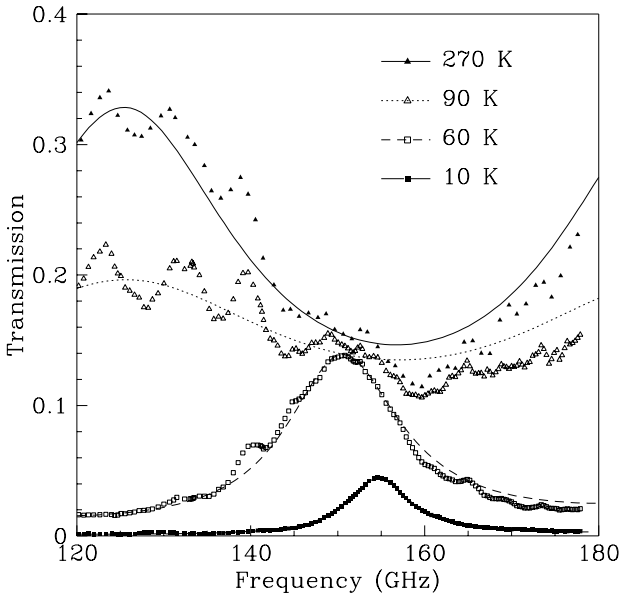

Figure 6.11: *Transmission of $DyBa_2Cu_3O_{7-\delta}$ on $LaAlO_3$ (thickness = 20 nm, T_c = 88 K) at 4 different temperatures together with their fit (10 K: solid squares, 60 K: open squares, 90 K: open triangles and 270 K: solid triangles).*

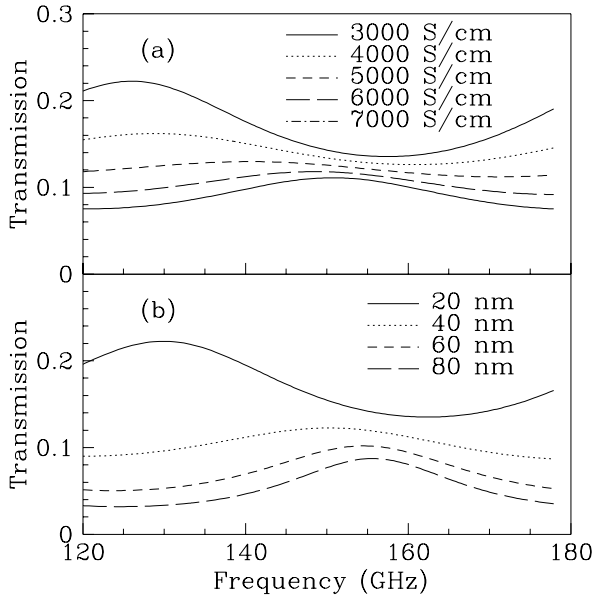

Figure 6.12: *Calculated transmission through a layered system (thin film on a substrate) as a function of conductivity (a) or thickness (b). For the substrate the optical constants of the $LaAlO_3$ were used ($\eta = 4.70$ and $\kappa = 0$), while the film thickness for (a) was 20 nm and the conductivity for (b) was 3000 $\Omega^{-1}cm^{-1}$.*

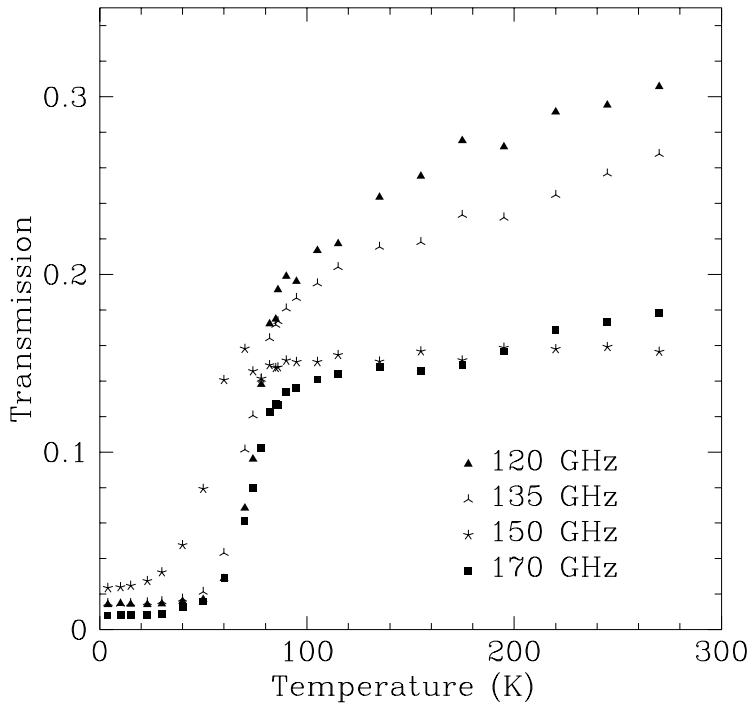

Figure 6.13: *Transmission as a function of temperature, at several fixed frequencies, clearly demonstrating the different behavior due to interference effects.*

tures as the 20 nm film (270, 90, 60 and 10 K). We see that the reduction in transmission at intermediate temperatures is much larger in the thicker film. As we will argue below, this is due to the stronger contribution of the superfluid in the 34 nm film. The transmission data for the 80 nm film, depicted in the inset of fig. 6.14, show qualitatively similar behavior as the 34 nm thick film.

Data Analysis, yielding σ_1 and ϵ'

To fit the transmission data presented in fig. 6.11 we use two different approaches. First we start in the normal state, knowing that there is no superfluid fraction present (approach A). This yields both ϵ' and ϵ'', where the sensitivity in the metallic case is most extensive for ϵ'' ($\sim \nu_{pn}^2/\gamma$). We continue this approach even when the sample is cooled below T_c where the addition of a superfluid contribution does not influence the fit for the 20 nm film significantly. We proceed until the peak becomes too narrow and fitting is no longer possible. The second approach (B) is to start at the lowest possible temperature (5 K) and assume that the superfluid fraction is the dominant contribution. We proceed to higher temperatures until the peak starts to broaden and the maximum remains nearly constant, thus inhibiting fitting with the superfluid as the only contribution. Obviously there will

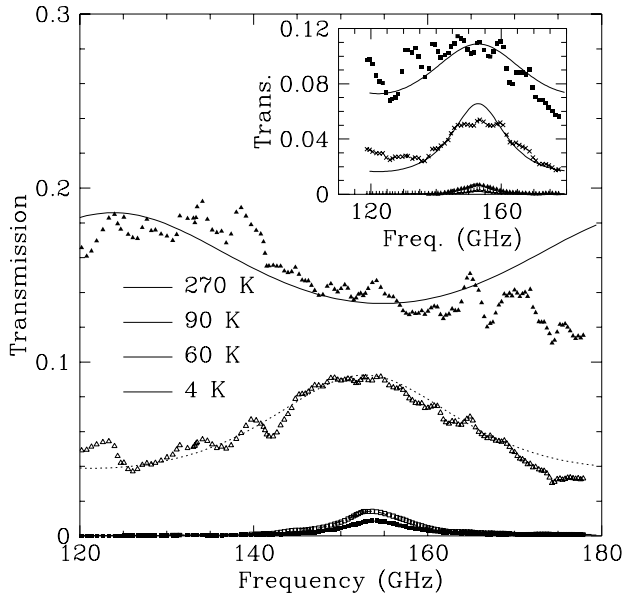

Figure 6.14: *Transmission of $DyBa_2Cu_3O_{7-\delta}$ on $LaAlO_3$ (thickness = 34 nm, T_c = 91 K) at 4 different temperatures (10, 60, 90 and 270 K) along with their fit. Inset: Transmission of $DyBa_2Cu_3O_{7-\delta}$ (d = 80 nm) at the same temperatures.*

be a temperature range for which both terms are comparable, in which case a quantitative description is more complicated.

In fig. 6.15 σ_1 is shown, while in fig. 6.16 the total ϵ', including the superfluid contribution, has been depicted. Both σ_1 and ϵ' have been determined at the center frequency, $\nu = 5$ cm^{-1}, using $\sigma_1 = \nu_{pn}^2\gamma(\nu(\nu^2 + \gamma^2))^{-1}$ and $\epsilon' = -\nu_{pn}^2(\nu^2 + \gamma^2)^{-1} - c^2(2\pi\nu\lambda)^{-2}$. To determine σ_1 we used the values for ν_{pn} and γ obtained from the fit following approach A. In the analysis for the normal state the transmission is determined by σ_1, i.e. ν_{pn}^2/γ in the case of a large scattering rate. In order to obtain an absolute value for γ we therefore needed to assume a value for ν_{pn}, which is expected to be temperature independent in the normal state. Using $\nu_{pn} = 8000\text{cm}^{-1}$, we obtained the values for γ presented in the inset of fig. 6.15. Below T_c σ_1 exhibits a rapid increase for all films. For comparison, the conductivity for a BCS-superconductor with a T_c of 88 K is included as the solid line. The conductivity was normalized to the value of σ_1 for 20 nm $DyBa_2Cu_3O_{7-\delta}$ film at 88 K. This emphasizes the strikingly different behavior of the high T_c superconductor. Similar behavior has been observed before in $YBa_2Cu_3O_{7-\delta}$ [17, 18], and is taken to be evidence of a rapidly suppressed scattering rate γ below T_c. Since, within the model used, $\sigma_1 \sim \nu_{pn}^2/\gamma$, two competing effects determine its temperature dependence. Below T_c the density of normal carriers will be reduced thereby reducing the plasma frequency, ν_{pn}, while the scattering of quasiparticles will also be reduced when the temperature is lowered. Having two different temperature dependencies produces a maximum in the conductivity.

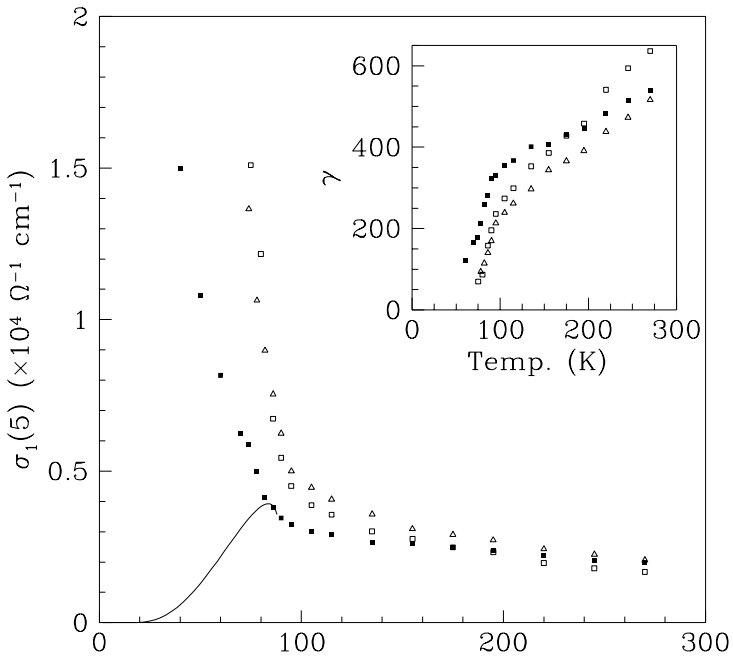

Figure 6.15: *Temperature dependence of σ_1 for three $DyBa_2Cu_3O_{7-\delta}$ films with different thicknesses (20 nm: solid squares, 34 nm: open triangles and 80 nm: open squares). The normalized conductivity for a BCS-superconductor having a T_c of 88 K is included as the solid line. The inset shows γ for all three films.*

This maximum also resembles, superficially, a BCS coherence peak but shows a different temperature and frequency behavior.

The total dielectric response, ϵ', is mainly determined by the superfluid contribution. For the 20 nm film ϵ' can not be determined accurately from 50 to 90 K, caused by the insensitivity of the transmission to ν_{ps} in this range. The solid curve in fig. 6.16 corresponds to an estimate of ϵ' based on the expression $\epsilon' = -2\sigma_1/\gamma$ which is valid for the Drude model.

Knowing the approximate values for the dielectric properties we return to our analysis in chapter 3, section 3.1.2 in order to show that the earlier claim that the sensitivity shifts from $\sigma_1(T)$ to $\lambda(T)$ in this temperature range was valid. Using equation (3.27) and the measured values for σ_1 and ϵ' we can calculate the critical thickness. The result can be seen in the inset in the fig. 6.16. Since the values used to calculate d_c are *intrinsic* material properties the curve looks similar when we use the dielectric properties obtained for the 34 and the 80 nm film. We can hence estimate at which temperature the critical thickness is approximately equal to the film thickness. These temperatures have been indicated in fig. 6.16 by three arrows, where the thinnest film is represented by the lowest temperature. Around these temperatures both approaches A and B are inefficient, resulting in a larger

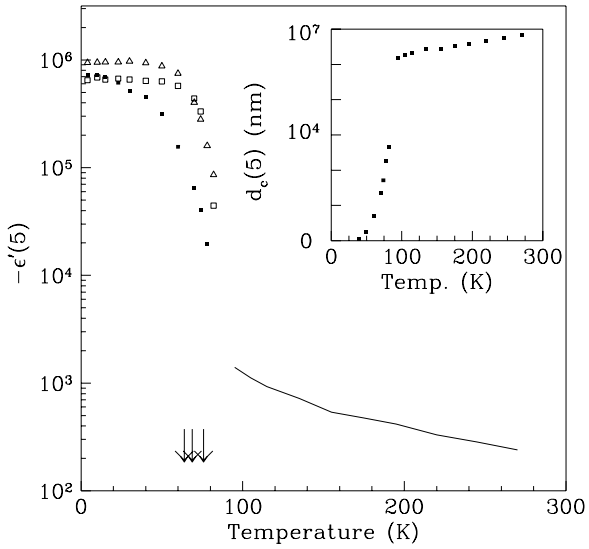

Figure 6.16: *Temperature dependence of ϵ' for three $DyBa_2Cu_3O_{7-\delta}$ films with different thicknesses (20 nm: solid squares, 34 nm: open triangles and 80 nm: open squares). The arrows indicate the temperatures where the critical thickness, d_c (inset), is approximately equal to the film thickness (20, 34 and 80 nm from left to right). The tentative line at higher temperatures shows the qualitative behavior calculated using the values for ω_{pn} and , obtained from σ_1. All quantities have been calculated at the center frequency, $\nu = 5\ cm^{-1}$.*

uncertainty in the obtained absolute values of both σ_1 and ϵ'.

Results for ρ_{dc} and λ(T)

More results of the fitting procedure are displayed in fig. 6.17 for all three films. The resistivity ρ is shown on the right hand side, while on the left hand side of fig. 6.17 the superfluid density $(\lambda(0)^2/\lambda(T)^2)$ is plotted. The results at low temperatures have been obtained using approach B. At higher temperatures ρ has been calculated by direct inversion of σ_1 obtained using approach A, assuming that σ_2 can be neglected. These results can be compared to the dc-resistivity depicted in fig. 6.18, which were obtained on samples prepared under identical conditions. The results show $\rho(300) = 650\,\mu\Omega$cm and $\rho(T_c) = 230\,\mu\Omega$cm, which is in good agreement with the mm-wave data in fig. 6.17. In the normal state the mm-wave data show a linear temperature dependence of the resistivity, similar to the dc-behavior. However, the slope tells us that there is a fairly large residual scattering. For instance for the 20 nm film the intercept at T = 0 K is about 225 $\mu\Omega$cm. Moreover, the slope is about twice as large as values measured for single crystals (1.05 $\mu\Omega$cm/K vs. 0.45 $\mu\Omega$cm/K), indicating that the difference cannot be explained by merely adding a temperature *in*dependent residual resistivity term.

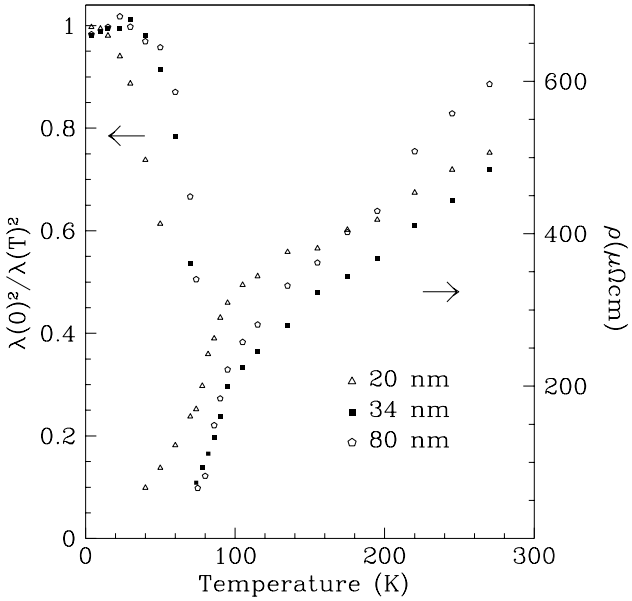

Figure 6.17: *Temperature dependence of the resistivity (right hand side) and the superfluid density* $\lambda(0)^2/\lambda(T)^2$ *(left hand side) for three* $DyBa_2Cu_3O_{7-\delta}$ *films with different thicknesses. (20 nm: solid squares, 34 nm: open triangles and 80 nm: open squares).*

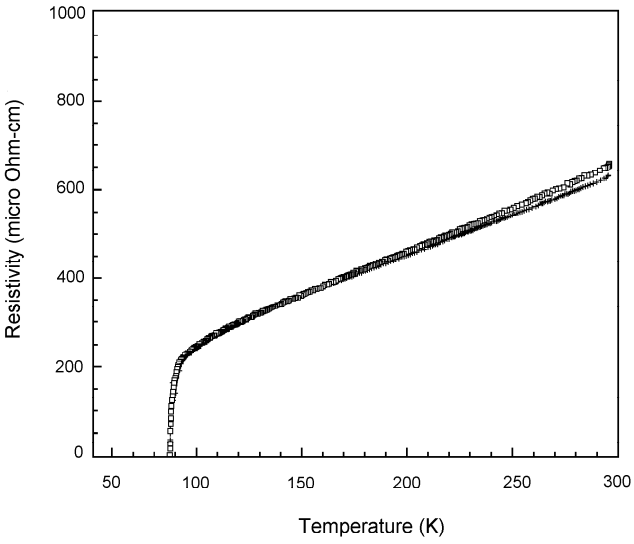

Figure 6.18: *dc-Resisitivity data taken on* $YBa_2Cu_3O_{7-\delta}$ *films prepared under identical conditions as the films used for the mm-wave transmission measurments.*

The absolute penetration depth of the 20 nm film is shown in fig. 6.19. as a function of T^2. The penetration depth shows a T^2-dependence at lower temperatures and a rather large

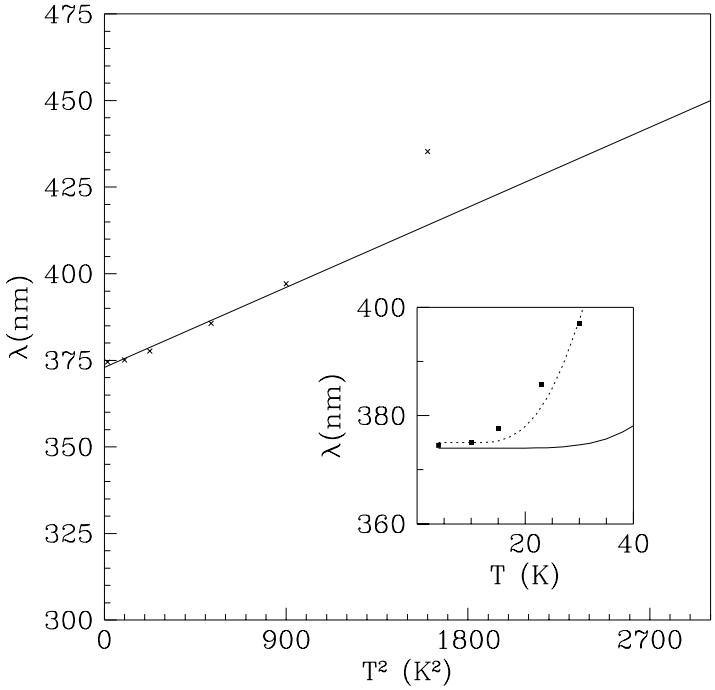

Figure 6.19: *The penetration depth for the 20 nm film vs. T^2. In the inset the penetration depth calculated using the BCS relations is shown along with the experimental data.*

λ_L of 370 nm. A strong objection to the interpretation of having a activated behavior can be seen in the inset, where the same results have been plotted together with a fit obtained a BCS-dependence [19].

$$1 - \left(\frac{\lambda(0)}{\lambda}\right)^2 = 2\pi \frac{e^{-\pi/\gamma\, t}}{\sqrt{2\gamma\, t}} \tag{6.2}$$

where $\pi/\gamma = \Delta/k_B T_c$ and $t = T/T_c$. We used several different values for the gap and obtained the "best" fit for $2\Delta/k_B T = 1.46$ (dashed line). The value for the BCS-ratio is rather small and disagrees with for instance tunneling and ARPES-data yielding values ranging from 4 to 7 [20, 21]. Also shown as the solid line is a fit using $2\Delta/k_B T_c = 2.76$, clearly demonstrating the inability to describe $\lambda(T)$ in this fashion. The factor 2.76 has been chosen in order to show the fashion in which the curvature changes when a larger gap ratio is chosen. An even more realistic choice, such as $2\Delta/k_B T_c = 3.74$ shows no temperature dependence in the plotted temperature range.

An interesting possibility might be that we are sensitive to the smallest of two gaps [22], however, at low temperatures the solution for the superconductor having an finite energy

gap tends to become temperature independent, whereas the measured values for λ still show an appreciable temperature dependence. The other films show similar behavior with a slightly different zero temperature penetration depth (325 and 360 nm for the 34 and 80 nm films respectively).

Similar behavior, having a correlation between a large absolute penetration depth and the quadratic temperature dependence was observed before by de Vaulchier *et al.* [5] and was taken to be evidence for the extrinsic nature of the temperature dependence, due to the existence of weak links within the film. This provides a more likely explanation for the observed T^2-dependence, namely the d-wave scenario, where the power-law temperature dependence of λ is lifted to a higher order by the presence of additional scattering [23]. The slope of the quadratic curve (~ 0.025 $\mathring{A}/K^2$) is about the same as that reported for one of the films in ref. [5], although due to the extrinsic nature of the phenomenon there is no need for these values to be the same.

6.5 Conclusions

We used mm-wave transmission as a complimentary technique to characterize and study superconducting thin films on a fundamental level. From the MoGe and the NbN-data we see that we are able to resolve the intrinsic behavior and obtain absolute values for both the real and imaginary part of the dielectric function. In both cases we can deduce values for σ_1 ($17,300$ and $15,000$ $\Omega^{-1}cm^{-1}$) and λ_L (500 and 400 nm). The temperature dependencies follow the expected BCS-behavior for transmission as well as the superfluid density $\lambda^2(0)/\lambda^2(T)$.

We have studied the transmission through $DyBa_2Cu_3O_{7-\delta}$ films of different thickness (20, 34 and 80 nm). We observed an enhanced conductivity in going into the superconducting state, indicative of a large reduction in the scattering rate γ just below T_c. For the resistivity in the normal state, we find the linear behavior typical for the cuprates. From the intercept at T = 0 K we learn that there is an additional residual scattering in the film, probably due to the same oxygen deficiency that reduces T_c slightly. The London penetration depth is fairly large for all films (325 - 370 nm), and has a T^2 dependence, consistent with a d-wave symmetry picture plus an additional extrinsic scattering source. For the thinnest film (20 nm), the superfluid density has no influence on the transmission coefficient down to temperatures well below T_c. Therefore the temperature dependence of the transmission is completely determined by σ_1, even at temperatures down to 60 K. The thicker films show a more conventional behavior, where ϵ' indeed dominates the transmission in most of the superconducting range.

References

[1] W. N. Hardy, D. A. Bonn, D. C. Morgan, Ruixing Liang and Kuan Zhang, Phys. Rev. Lett. **70**, 3999 (1993).

[2] Steven M. Anlage, Dong-Ho Wu, J. Mao, S. N. Mao, X. X. Xi, T. Venkatesan, J. L. Peng and R. L. Greene, Phys. Rev. B **50**, 523 (1994).

[3] T. Jacobs, S. Shridhar, C. T. Rieck, K. Scharnberg, T. Wolf and J. Halbritter, J. Phys. Chem. Solids **56** (12), 1945 (1995).

[4] for a complete reference on resonant cavity techniques see: O. Klein, S. Donovan, M. Dressel, K. Holczer and G. Grüner *Microwave Cavity Perturbation Technique: Part I, II and III*, International Journal of infrared and Millimeter Waves, **14**, 2423-2517 (1993).

[5] L. A. de Vaulchier, J. P. Vieren, Y. Guldner, N. Bontemps, R. Combescot, Y. Lemaître and J. C. Mage, Europhys. Lett. **33** (2), 153 (1996).

[6] J. Bardeen, L. N. Cooper and J. R. Schrieffer, Phys. Rev. **108** (5), 1175 (1957).

[7] R. E. Glover III and M. Tinkham, Phys. Rev. **104**, 844 (1956).

[8] D. M. Ginsberg and M. Tinkham, Phys. Rev. **118**, 990 (1960).

[9] J. M. Graybeal and M. R. Beasley, Phys. Rev. B **29**, 4167 (1984).

[10] Ali Yazdani, W. R. White, M. R. Hahn, M. Gabay, M. R. Beasley and A. Kapitulnik, Phys. Rev. Lett. **70**, 505 (1993).

[11] W. R. White, A. Kapitulnik and M. R. Beasley, Phys. Rev. Lett. **66**, 2826 (1991).

[12] D. G. Steel, W. R. White and J. M. Graybeal, Phys. Rev. Lett. **71**, 161 (1993).

[13] J. M. Graybeal, J. Luo and W. R. White, Phys. Rev. B **49**, 12923 (1994).

[14] D. C. Mattis and J. Bardeen, Phys. Rev. **111**, 412 (1958).

[15] M. Tinkham, *Introduction to Superconductivity*,
(McGraw-Hill, New York, 1975 and Krieger, New York, 1980).

[16] A. Shoji, S. Kiryu and S. Kohjiro, Appl. Phys. Lett. **60** (13), 1624 (1992)

[17] D. A. Bonn, P. Dosanjh, R. Liang and W. N. Hardy, Phys. Rev. Lett. **68**, 2390 (1992).

[18] Martin C. Nuss, P. M. Mankiewich, M. L. O'Malley, E. H. Westerwick and Peter B. Littlewood, Phys. Rev. Lett. **66**, 3305 (1991).

[19] B. Mühlslegel, Z. Phys. **155**, 313 (1959).

[20] Matthias C. Schabel, C.-H. Park, A. Matuura, Z. X. Shen, D. A. Bonn, Ruizing Liang and W. N. Hardy, Phys. Rev. B. **55**, 2796 (1997).

[21] for a review of tunneling experiments see for instance: Tetsuya Hasegawa, Hiroshi Ikuta and Koichi Kitazawa, Chapter 7 of *Physical Properties of High Temperature Superconductors, vol. III*, D. M. Ginsburg ed. (World Scientific, London, 1992), 525.

[22] N. Klein, N. Tellmann, H. Schulz, K. Urban, S. A. Wolf and V. Z. Kresin, Phys. Rev. Lett. **71**, 3355 (1993).

[23] P. J. Hirschfeld and N. Goldenfeld, Phys. Rev. B **48**, 4219 (1993).